Detection of Rotor Faults in Brushless DC Motors Operating Under Nonstationary Conditions

Satish Rajagopalan, *Member, IEEE*, José M. Aller, José A. Restrepo, *Member, IEEE*, Thomas G. Habetler, *Fellow, IEEE*, and Ronald G. Harley, *Fellow, IEEE*

***Abstract*—There are several applications where the motor is operating in continuous nonstationary operating conditions. Actuators and servo motors in the aerospace and transportation industries are examples of this kind of operation. Detection of faults in such applications is, however, challenging because of the need for complex signal processing techniques. Two novel methods using windowed Fourier ridges and Wigner–Ville-based distributions are proposed for the detection of rotor faults in brushless dc motors operating under continuous nonstationarity. Experimental results are presented to validate the concepts and illustrate the ability of the proposed algorithms to track and identify rotor faults. The proposed algorithms are also implemented on a digital signal processor to study their usefulness for commercial implementation.**

***Index Terms*—Condition monitoring, eccentricity, electric machines, nonstationary, rotor faults, spectrogram, Wigner–Ville distribution (WVD).**

I. Introduction

IN MANY applications, the electric motor operates under transient (nonstationary) conditions. The term nonstationary in the signal processing literature has a different connotation and is usually described statistically [1]. However, from an electric motor's operating point of view, this simply refers to an operation where the motor's operating points (speed and load) continuously change with time, and the motor is never operating at a constant speed throughout its operation. Such applications are commonly encountered in the aerospace, appliance, and automotive industries. An example of one such typical application is the use of electric motors in automotive actuators, which is the motivation behind this research. The diagnosis of motor health in such applications is critical to maintaining and improving process uptimes in industries or providing increased safety to humans. A segment of a permanent magnet brushless dc motor (BLDCM) stator current in a nonstationary state, representing an automotive actuator application, is shown in Fig. 1. Fig. 1 shows a brushless dc (BLDC) stator current snapshot sampled at 2 kHz and clearly depicts the simultaneously changing motor frequency and amplitude. In the nonstationary motor behavior under investigation in this paper, the electric motor operates in conditions shown in Fig. 1 throughout its operation.

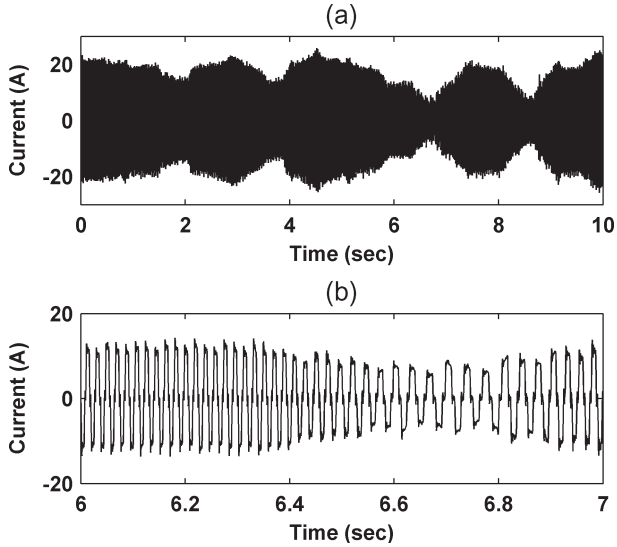

Fig. 1. (a) Nonstationary stator current in BLDCM. (b) Zoomed section of top plot depicting continuously changing motor frequency and amplitude.

The detection of faults in motors operating under constant speed conditions is straightforward because of the use of the well-known Fourier transformation [2]–[4]. However, the Fourier transformation cannot be directly applied to the analysis of nonstationary signals. This important limitation of the Fourier transformation raises the need for more sophisticated signal processing techniques for the analysis of nonstationary signals. Often, assumptions of local stationary operation may have to be made. Even under these assumptions, it is difficult to arrive at a solution that may be effective over a wide range of operating conditions and faults.

There has been little research in the area of fault diagnostics of motors operating under nonstationary conditions, and what has been reported is limited to induction motor applications. In one such method, the short time Fourier transforms (STFTs) and statistical methods are used to detect broken bar and bearing defects from the induction motor stator current in applications where the motor speed and load are time dependent. However, this algorithm is based on the assumption that the

Paper IPCSD-06-052, presented at the 2005 IEEE International Symposium on Diagnostics for Electrical Machines, Power Electronics and Drives, Vienna, Austria, September 7–9, and approved for publication in the IEEE TRANSACTIONS ON INDUSTRY APPLICATIONS by the Electric Machines Committee of the IEEE Industry Applications Society. Manuscript submitted for review November 19, 2005 and released for publication June 22, 2006. This work was supported by the Duke Power Company, Charlotte, NC.

S. Rajagopalan, T. G. Habetler, and R. G. Harley are with the School of Electrical and Computer Engineering, Georgia Institute of Technology, Atlanta, GA 30332 USA (e-mail: rsatish@ece.gatech.edu; thabetler@ee.gatech.edu; ron.harley@ece.gatech.edu).

J. M. Aller and J. A. Restrepo are with the Departamento de Conversión y Transporte de Energía, Universidad Simón Bolívar, Caracas 1080-A, Venezuela (e-mail: jaller@usb.ve; restrepo@usb.ve).

Digital Object Identifier 10.1109/TIA.2006.882613

changes in speed and load occur slowly, and there are sufficient intervals of time where the motor can be assumed to operate in a stationary condition [5]. Wavelet packet transforms and artificial neural networks have also been applied to detect motor faults in similar applications [6]. In [6], a residual is calculated by subtracting the output of a multistep ahead neuro-predictor from the actual current signal. The neuro predictor is developed using recurrent dynamic neural networks and predicts ahead of time the stator current of a healthy machine. A wavelet packet transform algorithm is then used to separate the different harmonics from the residual signal and to compute the fault indicators. Rather than use artificial neural networks, some researchers apply electrical models of induction motors to calculate the residual. For example, in [7], the researchers use a Park model of the squirrel cage induction drive to predict the behavior of a healthy motor. Here, a residual is calculated by subtracting the output of the Park model from the actual stator current. Wavelets are then used to process the residual. A threshold is set on the wavelet coefficients that are sensitive to motor faults, thereby allowing the detection of the motor faults. However, as rotor faults are small in magnitude, accurate neural network or electrical models are needed to separate the rotor fault information from the signal of the good motor. This limitation has been acknowledged in model-based algorithms that are more sensitive to stator faults than rotor faults, where rotor defects produce smaller changes in the stator current when compared to stator defects [7].

The use of wavelets to extract fault information from the stator current prior to classification has also been investigated, and reasonable success has been reported [8]. However, the problems of translation variance and the inability of discrete wavelets to closely approximate sinusoidal signals make their use difficult in rotor fault diagnostics [9].

Some researchers detect motor faults in induction motors by analyzing the starting current transient [10], [11]. This enables the detection of faults under a no-load condition where the only measurable and useful information exists in the large starting transient current of the motor. However, nothing has been published that attempts to diagnose faults in applications where the motor is continuously in a nonstationary state, or where assumptions of local or slow stationarity may be questionable and unrealistic. A detailed literature survey leads the authors of this paper to believe that fault feature extraction with a simple fault classification method is needed, and the extraction of fault features using time–frequency $(t-f)$ analysis is the most reasonable way to go forward.

The focus of this paper is to propose techniques that can be used to detect rotor faults in electric motors operating under continuously changing operating conditions. Therefore, this research is not limited only to the motor's startup condition. Two algorithms are proposed, namely: 1) a windowed Fourier ridge (WFR) algorithm and 2) a Wigner–Ville-variant-based algorithm. The WFR algorithm computes local maxima (or ridges) from the spectrogram of an adaptively filtered non-stationary motor current signal. The Wigner–Ville family of $t-f$ distributions is presented as a novel alternative to the WFR algorithm where enhanced detection of rotor faults may be required. The drawbacks of these distributions, and the methods to overcome them, are also presented. The proposed methods allow continuous real-time tracking of rotor faults in BLDCMs operating under continuous nonstationary conditions, thus allowing continuous monitoring of the motor health. The performance of both the methods are compared, and the practical implementation of these methods is also briefly discussed. Although the method could be readily generalized, its presentation is limited in this paper to BLDCMs.

II. Parametric Behavior of Rotor Faults in Nonstationary BLDCMs

Potential faults in BLDC machines can be categorized as stator faults, rotor faults, bearing faults, and inverter faults. The rotor faults could be because of eccentricities, unbalanced rotors, damaged rotor magnets, misalignments, and asymmetries [2]. The rotor eccentricities occur when there is an unequal air gap between the stator and the rotor and are classified into two main types, namely: 1) static and 2) dynamic, with the latter being the more severe of the two [2], [3]. If the eccentricity were to become large, the resulting unbalanced radial forces could cause the stator and rotor to rub, resulting in damage to both the stator and the rotor. In the case of the static air-gap eccentricity, the position of the minimal radial air-gap length is fixed in space. In the case of dynamic eccentricity, the center of the rotor is not at the center of rotation, and the position of the minimum air gap rotates with the rotor. The mechanically unbalanced rotor, a different kind of rotor fault, is usually caused by a misaligned load. This unbalance causes slight dynamic eccentricity and motor vibration, eventually leading to motor-bearing failure. Only two of the more common rotor faults, namely: 1) dynamic eccentricity and 2) mechanically unbalanced rotors, are used in this paper to develop the proposed fault detection methods and illustrate their viability. This is because of the difficulty in practically and accurately implementing all rotor faults in the laboratory. The proposed methods can be extended to other faults such as mixed eccentricities, misalignments, and asymmetries, as the behaviors of these other rotor faults are similar to the dynamic eccentricity and the unbalanced rotor faults.

A rotor defect such as dynamic eccentricity can be detected by monitoring certain characteristic fault frequencies in the electrical parameters of the BLDCM, namely the stator current [12], [13]. These frequencies, in the case of a constant speed motor operation, are given by

$$f_{\mathrm{rf}} = f_e \pm k\frac{f_e}{P/2} \tag{1}$$

where f_{rf} is the rotor fault frequency, f_e is the fundamental frequency, P is the number of poles in the BLDC machine, and k is any integer. The fault frequencies are also present when the current is nonstationary (dynamic motor operation). In such a case, the fault frequency components change in frequency and magnitude, depending on the operating point (speed and load) of the motor. These fault frequencies are tracked continuously over time using the proposed algorithms, which are explained in more detail in the subsequent sections.

III. WFRs and Wigner–Ville Distributions (WVDs)

A. WFRs

The windowed Fourier transform (WFT) was developed in 1946 when windowed Fourier atoms were introduced to measure the "frequency variations" of sounds. The WFT Sf of a function $f(t)$ is given by [14]

$$Sf(t,\xi) = \int_{-\infty}^{+\infty} f(\tau)g(\tau - t)e^{-i\xi\tau}d\tau \tag{2}$$

where $g(\tau)$ is a real and symmetric window translated by u and modulated by the frequency ξ, t is the instantaneous time, and τ is the "running time." This transform is also called the STFT because the multiplication by $g(\tau-u)$ localizes the Fourier integral in the neighborhood of $t = \tau$. The resolution in time and frequency of the WFT depends on the spread in time and frequency of the selected window type (Rectangle, Blackman, Hamming, Gaussian, Hanning, etc.). This spread is the smallest when the Gaussian window defined as follows is used [14]:

$$g(t) = e^{(-18t^2)}. \tag{3}$$

The WFT can be implemented digitally and efficiently in real time using discrete Fourier transforms (DFTs). The energy density possessed by the WFT is called a spectrogram denoted by $P_S f$ and is given by [14]

$$P_S f(t,\xi) = |Sf(t,\xi)|^2 = \left| \int_{-\infty}^{+\infty} f(\tau)g(\tau - t)e^{-i\xi\tau}d\tau \right|^2. \tag{4}$$

The spectrogram measures the energy of $f(t)$ in the $t-f$ neighborhood of (t,ξ).

The WFRs are the local maxima of the spectrogram that represent the instantaneous frequencies. The instantaneous frequency of any function $f(t)$ is defined as a positive derivative of the phase $\varphi'(t) \geq 0$, where φ is the phase of $f(t)$ [14]. If the signal $f(t)$ has only one frequency component, then the instantaneous frequency is $\xi(t) = \varphi'(t)$, and the amplitude a can be calculated by

$$a(t) = \frac{2\,|Sf\,(t,\xi(t))|}{\sqrt{s_l}\,|\hat{g}(0)|} \tag{5}$$

where s_l is the length, and $\hat{g}(w)$ is the Fourier transform of the window $g(t)$. If $\Phi_S(t,\xi)$ is the complex phase of $Sf(t,\xi)$, then it can be shown that the ridge points are points of stationary phase [14] since

$$\frac{\partial \Phi_S(t,\xi)}{\partial t} = \varphi'(t) - \xi = 0. \tag{6}$$

The ridge algorithm thus computes the instantaneous frequencies of a signal $f(t)$ from the local maxima of $P_S f(t,\xi)$. This approach is introduced by Delprat *et al.* to analyze musical sounds [15].

The practical implementation of the ridge algorithm is given as follows. Generally, the number of instantaneous frequencies is unknown. In such cases, all local maxima of $P_S f(t,\xi)$, which are also points of stationary phase, are calculated. These points define curves in the (t,ξ) planes that are the ridges of the WFT. Ridges that have small amplitudes are often removed because they can be artifacts of noise variations or "shadows" of other instantaneous frequencies created by the sidelobes of $\hat{g}(w)$. If the signal consists of only a few frequencies, then all the local maxima are themselves the ridges and can be checked by computing the stationarity of their phases using (6). The ridges will be distinct as long as the distance between any two instantaneous frequencies (i.e., φ_1' and φ_2') satisfies [14]

$$|\varphi_1'(t) - \varphi_2'(t)| \geq \frac{\Delta w}{s_l} \tag{7}$$

where Δw is the bandwidth of the window.

B. WVD and Its Variants

$t-f$ analysis consists of the three-dimensional time, frequency, and amplitude representation of a signal, which is inherently suited to indicate transient events in the signal. The Wigner distribution and its various permutations is an analysis technique that has been widely used in the detection of faults in mechanical systems, the most common being the gear train. The WVD is derived by generalizing the relationship between the power spectrum and the autocorrelation function for nonstationary time-variant processes. The WVD of a signal $s(t)$ is given by [16]–[18]

$$W(t,\omega) = \frac{1}{2\pi}\int_{-\infty}^{\infty} e^{-j\omega\tau} s^*\left(t - \frac{\tau}{2}\right) s\left(t + \frac{\tau}{2}\right) d\tau \tag{8}$$

where s^* is the conjugate of s, and ω is the instantaneous frequency. The frequency ω is similar to the instantaneous frequency ξ but has been given a different symbol to differentiate the fact that ξ is obtained from the positive phase derivative. The WVD is part of a more general distribution called the Cohen class of generalized $t-f$ distributions $\rho(t,\omega)$ [16] given by

$$\rho(t,\omega) = \frac{1}{4\pi^2}\iiint e^{j\theta(u-t)}\phi(\theta,\tau)s^*\left(u - \frac{\tau}{2}\right) \times s\left(u + \frac{\tau}{2}\right) e^{-j\omega\tau} d\theta\, du\, d\tau \tag{9}$$

where $\varphi(\theta,\tau)$ is an arbitrary function called the kernel. Setting the kernel $\varphi(\theta,\tau) = 1$ yields the well-known WVD. It is a high-resolution technique offering much better frequency resolution than the STFT [19]. Moreover, the distribution can be used for the analysis of nonstationary signals without any underlying assumptions.

The WVD is a biquadratic distribution and produces large undesirable frequency components called cross terms that can hamper the interpretation of the distribution. Ghosts and artifacts are also produced. However, these are usually smaller in magnitude and can be removed by thresholding. These cross terms are significantly larger in amplitude when compared to the actual spectral components (also called as autoterms) in the signal. There are several variants of the WVD that attempt to

suppress such cross terms, and the two prominent ones are listed as follows:

1) pseudo-WVD (PWVD);
2) smoothed PWVD (SPWVD).

The PWVD is the windowed version of the WVD. The PWVD may be defined in the time domain or in the frequency domain, although the former is more common. Also called the windowed Wigner distribution, the PWVD suppresses cross terms present in the original Wigner distribution and has better resolution than the STFT [19]. The PWVD is defined as

$$W_P(t,\omega) = \frac{1}{2\pi}\int_{-\infty}^{\infty} e^{-j\omega\tau} h(\tau) s^*\left(t-\frac{\tau}{2}\right) s\left(t+\frac{\tau}{2}\right) d\tau \tag{10}$$

where $h(t)$ is the time-smoothing window.

The SPWVD uses a function that smoothes the distribution in both the time and frequency planes. The SPWVD offers better cross-term suppression though at the cost of frequency resolution. This smoothing function is usually Gaussian but smoothing windows such as Hamming can also be used. The SPWVD is given by [16]

$$W_S(t,\omega) = \int_{-\infty}^{\infty} L(t-t',\omega-\omega') W(t',\omega') dt' d\omega' \tag{11}$$

where L is the chosen smoothing window (usually Gaussian) applied to the WVD $W(t,\omega)$. t' and ω' are time and frequency variables respectively over which the smoothing is carried out. The Gaussian smoothing function is given by

$$L(t,\omega) = \frac{1}{\alpha\beta} e^{\frac{-t^2}{\alpha} - \frac{\omega^2}{\beta}} \tag{12}$$

and it has been known for a long time in quantum literature that for certain values of α and β, a positive distribution is obtained with many of the artifacts suppressed [16]. The condition to be satisfied to obtain such a positive distribution is

$$\alpha\beta \geq 1. \tag{13}$$

IV. Comments on Frequency Resolution of WFT- and WVD-Based Distributions

To illustrate the performance of the aforementioned signal processing techniques, a test signal i_a, approximating a rotor fault and having a fundamental of amplitude 0.05 A (corresponding to a filtered stator current) with two rotor fault sidebands of amplitude 0.07 A, is generated using

$$i_a = 0.05\cos(2\pi p(t)t) + 0.07\cos(4\pi p(t)t/3) + 0.07\cos(8\pi p(t)t/3). \tag{14}$$

The three frequencies in (14) are the fundamental frequency $p(t)$ and two rotor fault frequencies at 2/3rd and 4/3rd of the fundamental frequency $p(t)$. A 1-s record with 2048 samples is used for comparing the various signal processing techniques. The amplitudes in (14) are chosen arbitrarily to imitate a rotor fault scenario as close as possible. The frequency $p(t)$ is varied sinusoidally between 0 and 120 Hz as

$$p(t) = \sin(2\pi f t) \tag{15}$$

where $f = 120$ Hz.

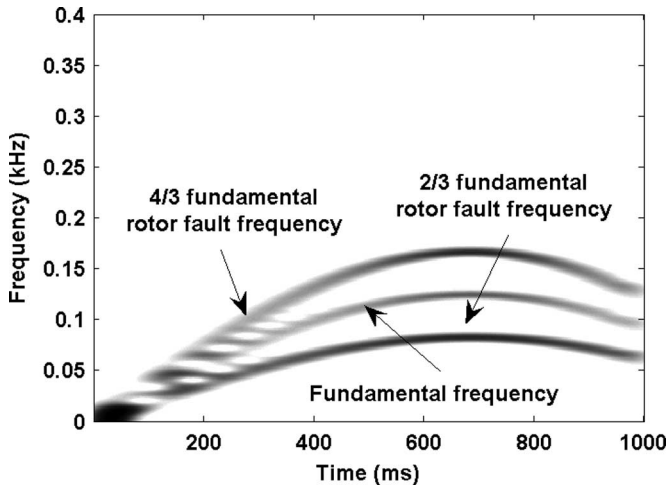

Fig. 2. WFT of simulated BLDCM rotor fault using hypothetical test signal i_a.

The choice of a windowing function can play an important role in determining the quality of the overall results. The main role of the window is to damp out the effects of the Gibbs phenomenon that results from truncation of an infinite series [20], [21]. Different windows offer different tradeoffs between the ability to offer good frequency resolution and introduction of undesired artifacts (Gibbs phenomenon) [20], [21]. In the $t-f$ analysis, the window also affects the time resolution along with the frequency resolution [14]. The Gaussian window provides the best compromise between the time and frequency resolutions and is used in the WFT computations in this research [14]. In addition, the length of the window plays a critical role, too. The window length is chosen as 0.25 s. This length is chosen through trial and error to obtain a good frequency resolution while simultaneously maintaining time resolution. A larger window length produces a smaller frequency resolution while not providing any significant improvement in the time resolution. Similarly, a shorter time window provides a marginally improved frequency resolution while reducing the time resolution. Fig. 2 shows the two-dimensional $t-f$ plot of the spectrogram (WFT) of the test signal computed using (4). The $t-f$ plot of Fig. 2 describes the variation of the three frequencies (y axis) in the signal i_a over time (x axis). The rotor fault frequencies at 2/3rd and 4/3rd of the fundamental frequency, along with the fundamental itself, are seen to be distinctly tracked over time in Fig. 2, except in the low-frequency region of 0–50 Hz. The frequency resolution is reduced at low frequencies, and this is expected because of the relatively short window length. Fig. 2 shows that the frequency components of the stator current waveform of a faulty BLDCM can still be distinctly detected over a wide frequency range using the WFT.

The Rice University Time Frequency Analysis toolbox [22] for MATLAB is used to compute the Wigner distributions for the simulated motor current signal. This toolbox has specific

functions tailor made for $t-f$ analysis. However, there are two significant problems that arise when applying the WVD or its variants to diagnose rotor faults in BLDCMs, which are listed as follows.

1) Interaction between the fundamental frequency and the fault frequencies in (14) produces cross terms at the same values as some fault frequencies produced by (1). These cross terms may be difficult to suppress even using the PWVD or the SPWVD, as the fundamental frequency is several orders of magnitude larger than the fault components, resulting in large cross terms.
2) The WVD spectrum of a real-valued signal has both a positive and a negative frequency part in the WVD spectrum, and this produces cross terms between the negative and the positive frequencies. The stator current, being a real-valued signal, suffers from this problem. These cross terms can be eliminated by eliminating the negative frequency terms.

The problem in 1) can be solved by adaptively filtering the fundamental and other inverter harmonics. In motors with large numbers of poles, certain harmonics may be selectively filtered (using an adaptive comb filter) prior to any signal processing. Thus, the cross terms that may occur at the motor fault frequencies can be avoided. The PWVD or SPWVD can then be used to suppress any remaining cross terms that may be produced because of the interaction with the fundamental.

The negative frequency terms that are mentioned in 2), as well as other artifacts, can be removed by converting the real-valued signal to an analytic version of the same by using the Hilbert transform. The use of the analytic signal also eliminates the need to sample at twice the Nyquist rate [19]. The analytic signal of a real-valued signal $s(t)$ can be defined as

$$s_A(t) = s(t) + j s_H(t) \tag{16}$$

where $s_H(t)$ is the Hilbert transform of the signal $s(t)$ and is given by

$$H\left[s(t)\right] = s_H(t) = \frac{1}{\pi}\int_{-\infty}^{\infty} s(\tau)\frac{1}{t-\tau}d\tau. \tag{17}$$

The Fourier transform $S_A(f_a)$ (where f_a is the Fourier transformed frequency) of the analytic signal in (16) does not possess negative frequency components as shown in (18), where $S(f_a)$ is the Fourier transform of $s(t)$, and $S_H(f_a)$ is the Fourier transform of $s_H(t)$. That is

$$\begin{aligned} S_A(f_a) &= S(f_a) + jS_H(f_a) \\ &= S(f_a) + \operatorname{sgn} f_a S(f_a) \\ &= \begin{cases} 0, & \text{if } f_a < 0 \\ S(f_a), & \text{if } f_a = 0 \\ 2S(f_a), & \text{if } f_a > 0 \end{cases}. \end{aligned} \tag{18}$$

A Gaussian window of length 0.25 s is used to suppress the cross terms in all the WVD-based distributions. The frequency resolution of the WVD-based distributions is superior to a WFT in spite of the use of a window function. This has been well documented [19] and will be demonstrated here. The length is again chosen through trial and error to obtain the best possible $t-f$ resolution. Fig. 3 is a $t-f$ plot that shows the PWVD of the signal obtained using (10). The PWVD offers much better frequency resolution than the WFT at low frequencies but suffers from the problem of cross terms. However, the SPWVD in Fig. 4 offers complete suppression of the cross terms while still offering better frequency resolution than the WFT. The PWVD and the SPWVD are calculated for the analytic version of the real-valued motor current signal. The analytic signal is obtained from the real-valued current signal i_a in (11) using (16) and (17).

Moreover, Fig. 2 also shows that the spectral components produced by the WFT are smeared in the frequency domain. Hence, the fault frequencies are not localized but spread over a frequency range. The PWVD and the SPWVD $t-f$ plots in Figs. 3 and 4 show a better concentration of energy in the frequency domain. This allows the PWVD and the SPWVD to provide a more accurate indication of the fault harmonic amplitudes when compared to the WFT.

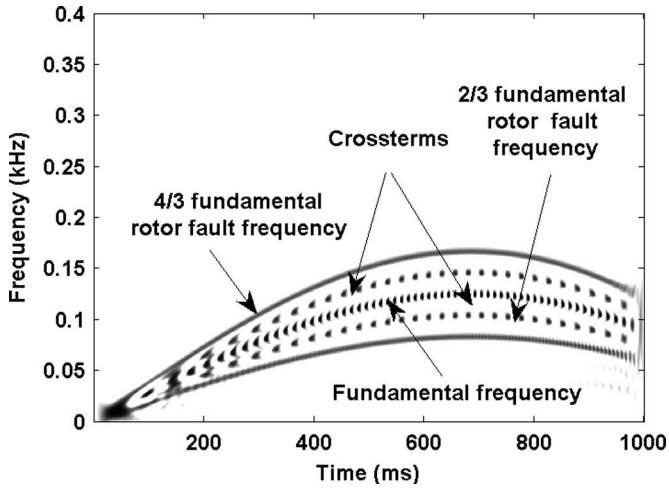

Fig. 3. PWVD of simulated BLDCM rotor fault using hypothetical test signal i_a.

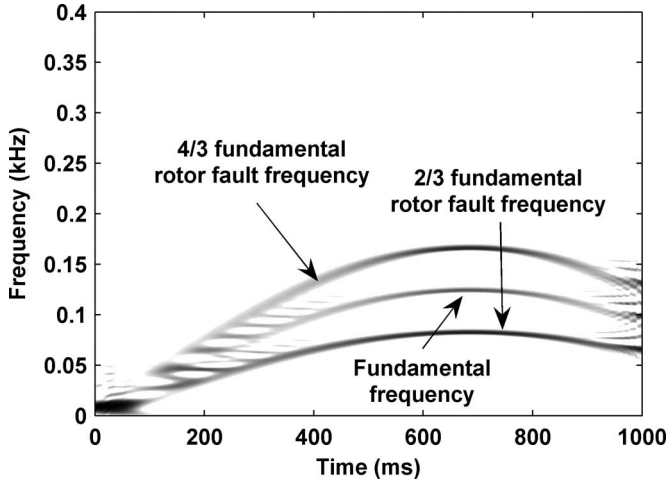

Fig. 4. SPWVD of simulated BLDCM rotor fault using hypothetical test signal i_a.

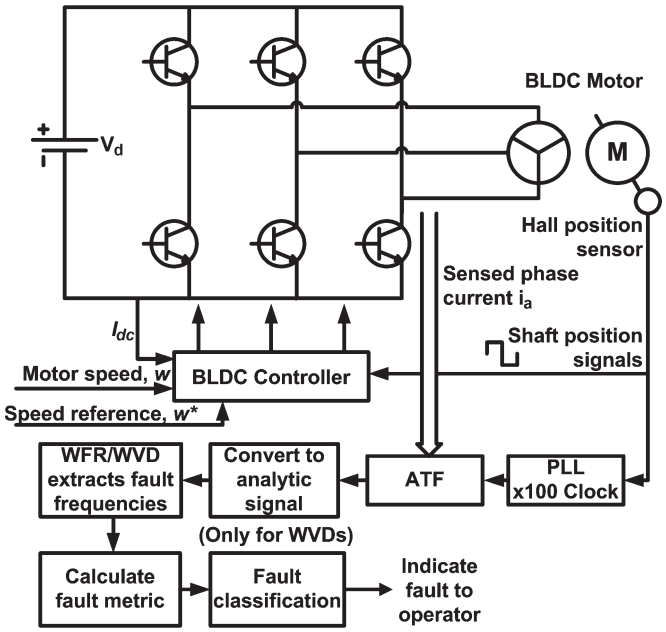

Fig. 5. Rotor fault detection in BLDCMs operating under nonstationary conditions.

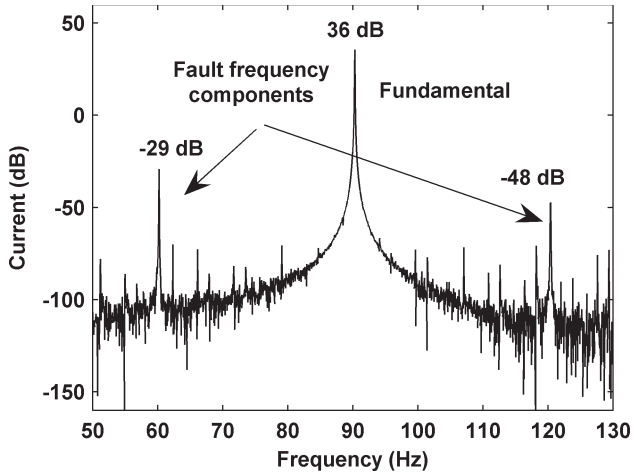

Fig. 6. Attenuation of fault sidebands with respect to fundamental for case of BLDCM with dynamic eccentricity.

However, the price paid for this superior performance of the SPWVD is increased computation complexity as will be shown.

V. Proposed Fault Detection Algorithms

A block schematic of the proposed algorithm is shown in Fig. 5. First, the fundamental and harmonics greater than two are adaptively filtered using an analog switch capacitor tracking filter (ATF). This is necessary as the fault frequency components are small in comparison to the amplitude of the fundamental and its harmonics. As an illustration, Fig. 6 depicts the relative magnitude of the fault frequency sidebands with respect to the fundamental for the case of a BLDCM with dynamic eccentricity operating at about 30% of full load. It can be seen that the fault sidebands are really small at about 80–90 dB below the peak of the fundamental amplitude. The filtering also decreases the occurrence of cross terms when using quadratic distributions such as the SPWVD, as explained in Section IV.

Every motor has some small abnormality from the time of manufacture, and the motor stator current has some fault frequency components. Hence, in all the condition monitoring algorithms, base measurements are taken for a good motor prior to commissioning. Once commissioned, the fault algorithm monitors the amplitudes of the fault frequencies and tracks the changes in their amplitudes over time. A significant change in the fault frequency amplitudes indicates a developing fault.

Two algorithms are proposed—one based on the WFRs and one based on PWVD/SPWVD. Each method has its own benefits and drawbacks, which are compared in this paper. A description of the implementation of each of the fault detection algorithms is given in the following sections.

A. WFR-Based Fault Detection Algorithm (Method 1)

First, a spectrogram is obtained using (4) from the filtered current signal. The Fourier ridges (amplitudes of the instantaneous frequencies of the spectrogram) are then extracted from the spectrogram by detecting the local maxima. A simple fault metric is then calculated by calculating the root mean square (rms) value of the instantaneous amplitudes of the fault ridges (local maxima of the spectrogram) and is given by

$$\text{RMS Fault Metric} = \sqrt{\frac{1}{N_r}\sum_{i=1}^{i=N_r} f_i^2(t)} \tag{19}$$

where $f_i(t)$ is the amplitude of the instantaneous rotor fault frequencies extracted from the spectrogram of the filtered current using the ridge algorithm. The N_r in (19) corresponds to the number of Fourier ridge frequencies extracted at any given time. This metric is used to indicate a developing rotor fault. Thresholds are set to determine the severity of the fault and provide an indication to the operator to take the necessary precautionary action. As the fault frequency magnitudes are dependent on the instantaneous speed and load conditions, automatically, variable thresholds are set to vary with load and speed conditions.

B. WVD-Based Fault Detection Algorithm (Method 2)

The filtered stator current is first converted into an analytic signal using the Hilbert transformation explained in the previous section [see (16) and (17)]. The SPWVD or the PWVD is then calculated for a time slice of predetermined length on the Hilbert-transformed analytic current signal using either (10) or (11), depending on the chosen method. The length is usually a power of two to facilitate fast computation. The fault frequencies obtained from the SPWVD/PWVD calculation are then used to compute a fault metric that indicates the health of the motor. A simple rms-fault-based metric is then used for fault classification and is given by (19).

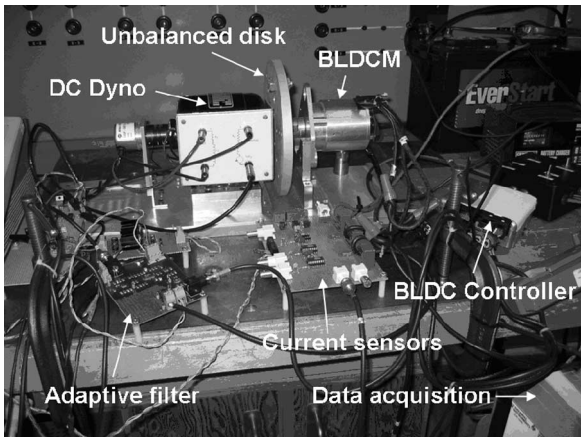

Fig. 7. Experimental arrangement to test fault detection in dynamically operating BLDCMs.

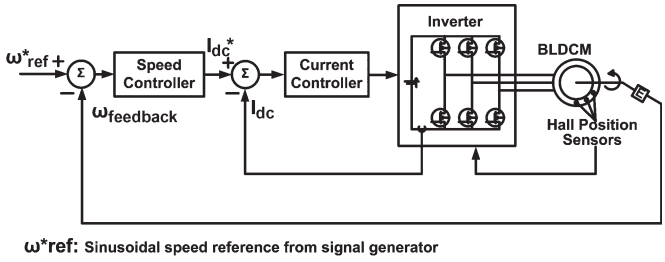

Fig. 8. Detailed block diagram of BLDCM controller.

VI. Experimental Results

The experimental setup is shown in Fig. 7. A 12-V 1-kW six-pole BLDCM with surface mount magnets is coupled to a dc generator that acts as a load. The BLDCM is driven by an inverter that features an integrated current control loop. The inverter is supplied from a 12-V deep-cycle lead-acid battery. An analog speed controller designed at the Georgia Institute of Technology is used to control speed. A detailed block diagram of the BLDCM controller is shown in Fig. 8. The speed signal is provided by a 1000 ppr optical encoder coupled to the dc generator. Hall effect sensors are used to sense the motor stator currents. One of the sensed phase currents is passed through the ATF as shown previously in Fig. 5. The filtered current as well as the raw input current is acquired using a 16-b data acquisition system.

Two filter systems, i.e., ATF1 and ATF2, are developed. A test ATF (ATF1) with a notch depth of 30 dB was initially prototyped on a vector board and is also used in some of the experiments. The ATF1 was subsequently improved and fabricated on a four-layer printed circuit board to obtain noise-free performance. A block diagram of both the ATFs is shown in Fig. 9 and consists of the following four components: 1) a digital phase-locked loop (PLL) clock; 2) a fixed-frequency analog Butterworth low-pass filter; 3) a switch capacitor variable frequency elliptic notch filter; and 4) a switch capacitor variable frequency Butterworth low-pass filter. The ATF removes the fundamental and all frequencies greater than the second harmonic. The fourth-order Butterworth low-pass filter is a fixed-frequency analog prefilter that provides antialiasing by removing all high-frequency components such as the pulsewidth

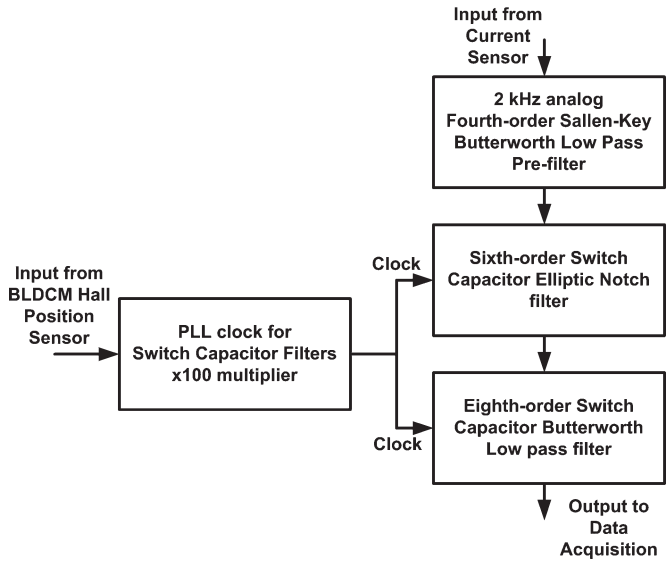

Fig. 9. Block diagram of ATF.

modulation frequencies of the BLDC drive. The notch filter, which removes the fundamental, is a sixth-order Elliptic switch capacitor filter designed using the software FilterCAD from Linear Technologies. The sixth-order filter is implemented using the LTC1061 high-performance triple universal integrated circuit. The ratio of the 0-dB width to the notch width is 10 : 1, with a notch attenuation of 56 dB. An eighth-order Butterworth low-pass switch capacitor filter is then used to filter out all harmonics above the second harmonic. The low-pass switch capacitor filter is implemented using a monolithic eighth-order filter chip MAX295 from Maxim. A low-pass attenuation of well over 80 dB is achieved. The MAX295 has an uncommitted operational amplifier that is used to finally amplify the filtered signal prior to data acquisition. The passband ripple is limited to less than 100 mdB. A simple resistance–capacitance postfilter removes clock feed through. Clocking for the filter is obtained from the BLDCM's Hall position sensors using a digital PLL that tracks the fundamental frequency of current.

For a six-pole BLDCM, the rotor fault frequencies occur at 1/3rd, 2/3rd, 4/3rd, and 5/3rd times the fundamental frequency as computed from (1). Rapid time-varying motor operation is obtained by varying the speed reference as shown in Fig. 5. Experiments are conducted with sinusoidal, triangular, and randomly changing speed references. The sinusoidal and triangular references are varied between 0 and 15 Hz, representing most practically occurring applications. For example, the sinusoidal reference changes as

$$\omega^*_{\mathrm{ref}} = 5\sin(2\pi f_{\mathrm{ref}} t) \tag{20}$$

where f_{ref} is a frequency between 0 and 10 Hz. The values of f_{ref} selected for these experiments are 3, 5, 8, 10, 12, and 15 Hz. The frequencies are selected to uniformly span over the range of 0–15 Hz.

A signal generator is used to provide the sinusoidal and triangular reference signals. The motor speed varies in the range of 600 to 1800 rpm. Two fault cases are presented here, namely 1) a mechanically unbalanced rotor and 2) a dynamically eccentric rotor.

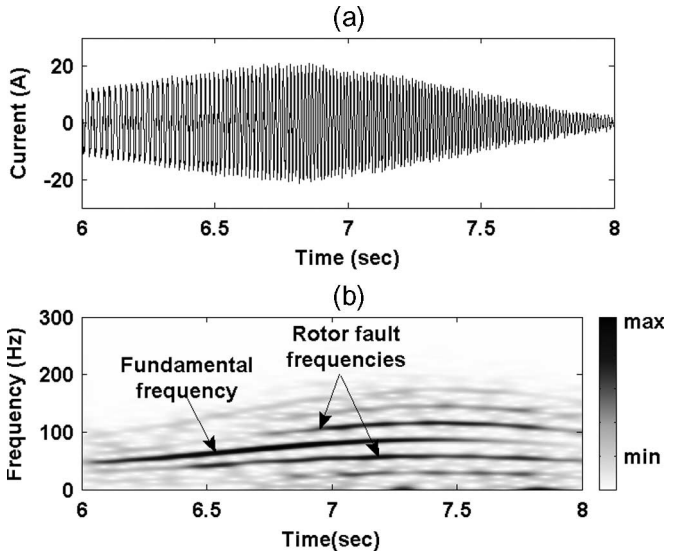

Fig. 10. Nonstationary BLDCM stator current and spectrogram of corresponding filtered BLDCM (with mechanically unbalanced rotor) stator current with 3-Hz sine speed reference.

A. Mechanically Unbalanced Rotor

A mechanically unbalanced rotor is implemented by mounting a slotted disk on the shaft of the motor (Fig. 7). The level of unbalance can be changed, depending on the position of the bolt in the slots on the disk. Such an unbalanced disk causes slight unbalance on the rotor shaft besides vibration and pulsating torques. The test ATF (ATF1) with a 30-dB notch is used in this experiment to remove the fundamental frequency and all frequencies above the second harmonic.

Method 1 is applied first. The acquired data are divided into sections of 2 s each. The data are sampled at 2 kHz, and a Gaussian window of length 0.25 s is used to compute the spectrogram using (4). This window length is chosen through trial and error to obtain the best compromise between frequency and time resolution. A dc generator load is used for the BLDCM. This provides full load torque to the BLDCM at rated speed. The full load stator current for the BLDCM is 20 A.

The stator current of a mechanically unbalanced BLDCM (with a bolt in one of the disk slots) operating with a 3-Hz sinusoidal speed reference is shown in Fig. 10. The spectrogram of the filtered stator current calculated using (4) is also shown in Fig. 10. The fault frequencies are still not distinctly visible as the spectrogram extracts all spectral components including noise from the filtered current. The instantaneous fault frequencies or fault ridges are now extracted from the local maxima of the spectrogram by testing all extracted maxima for stationary phase using (6). Thus, only the fault ridges (instantaneous fault frequencies) are extracted from the filtered current and are shown in Fig. 11. The Fourier ridge algorithm is implemented in the Wavelab toolbox from Stanford University [23]. This toolbox provides functions for computing the ridges that are not present in the commercial toolbox that accompanies MATLAB. A fundamental component is also present in the extracted ridges of Fig. 11, as the 30-dB ATF1 used here does not remove the fundamental frequency component completely.

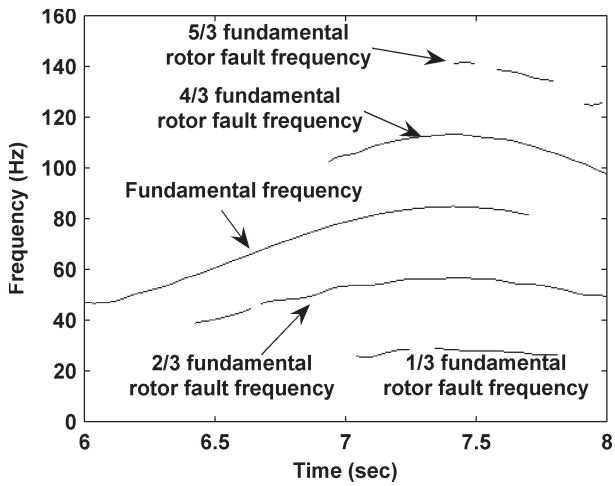

Fig. 11. Windowed Fourier ridges of filtered BLDCM (with a mechanically unbalanced rotor) stator current and 3-Hz sine speed reference.

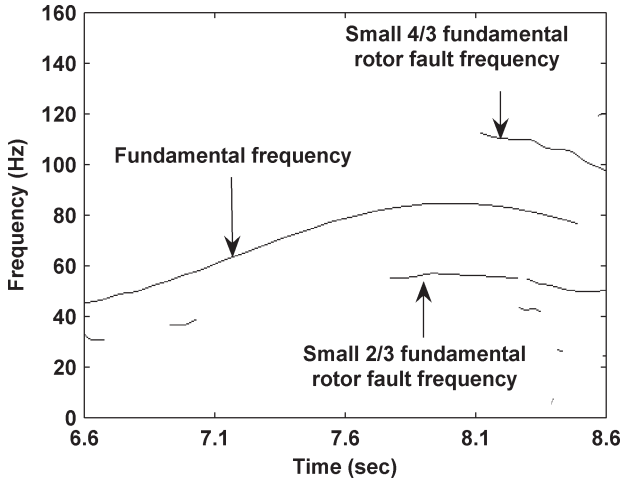

Fig. 12. Windowed Fourier ridges of filtered BLDCM (with mechanically balanced rotor) stator current and 3-Hz sine speed reference.

The bolt on the disk is now removed to obtain a mechanically balanced motor, and the experiment is repeated with the same 3-Hz sinusoidal speed reference. All other conditions remain the same. The WFRs of the filtered current for this case are shown in Fig. 12. The segment of current analyzed in Fig. 12 is selected to be similar to the one used in Fig. 7. A fundamental component is again present in Fig. 12 because of the reasons mentioned earlier. Even without the bolt, the disk comprises a slight unbalance by itself, and some fault harmonic frequencies are present, but these are smaller than the case with a bolt on the disk as shown previously in Fig. 11.

B. Dynamic Eccentricity

As mentioned earlier, in dynamic eccentricity, the center of the rotor is not at the center of the stator, and the position of minimum air gap rotates with the rotor. This misalignment may be caused by several factors such as misalignment of bearings, mechanical resonance at critical speeds, a bent rotor shaft, or wear of bearings. An actual dynamic eccentricity is implemented in the laboratory. One end of the rotor is first removed from the bearing. This end is selected as the one

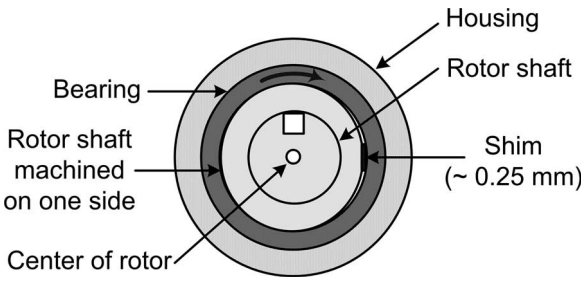

Fig. 13. Laboratory implementation of dynamic eccentricity

opposite to the end that houses the Hall position sensors in order not to disturb these sensors. In a machine shop, the material is removed from one side of the rotor shaft at the nonsensor end of the motor, and the rotor is then placed back onto the bearing. Shims are now inserted between the bearing and the shaft on the side opposite to where the material was removed as shown in Fig. 13, thus pushing the center of rotation of the rotor away from the center of the stator.

The original length of the air gap was 0.75 mm, and the rotor is now shifted by approximately 0.25 mm (32% of normal air-gap length) from its center by inserting a steel shim of thickness 0.001 in (∼0.25 mm). The defect induced in this manner represents a realistic dynamic eccentricity fault that can occur during normal motor operation.

Typical recommended eccentricity tolerances during manufacture are usually in the range from 5% to 20% of variation in the air gap [24]. A dynamic eccentricity of 32% change in the air gap is usually moderate and is, therefore, chosen for this study to depict the ability of the proposed algorithms to detect even moderate fault conditions. Motors with 32% eccentricity have run with barely detectable abnormal vibration levels at the Georgia Institute of Technology. As the proposed algorithms are signal processing methods akin to the standard FFT, the sensitivity of these methods is not different from the sensitivity of an FFT under steady-state conditions. This aspect is well documented in the literature [3].

The data are again sampled at 2 kHz, and a Gaussian window of length 0.25 s is used. The motor is tested under load conditions that vary from full load to low load, depending on the instantaneous speed of operation. Method 1 is first investigated. The WFRs (instantaneous fault frequencies) of the filtered stator current of a motor with dynamic eccentricity and operating with a 3-Hz sinusoidal speed reference are shown in Fig. 14. These Fourier ridges are extracted from the spectrogram of the filtered current signal using (4). The 56-dB ATF2 explained in detail in Section V is now used in this experiment. As the fundamental has been almost completely suppressed, the ridge algorithm detects and tracks only the fault frequencies.

The Fourier ridges in Fig. 14 are determined to be the fault frequencies at 2/3rd and 4/3rd the fundamental frequency by comparing them with Fourier ridge of the unfiltered signal that predominantly consists of only the fundamental component (Fig. 15), as the fault frequencies are ignored as noise in relation to the fundamental component. A Gaussian window of length 0.25 s is used. The data are processed in MATLAB using the Wavelab802 toolbox. The fault frequencies are seen to be tracked over time.

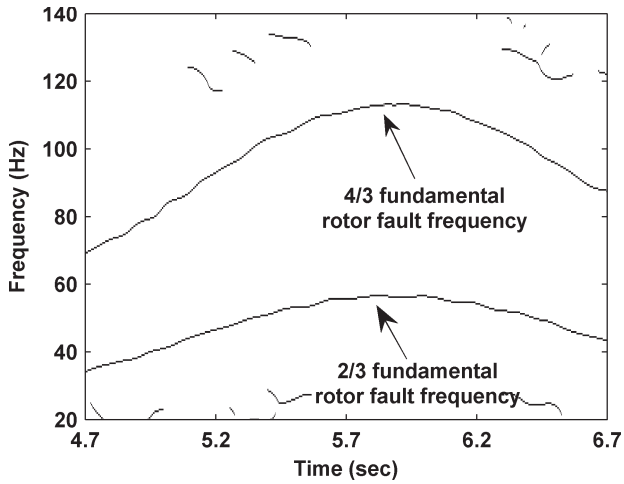

Fig. 14. Windowed Fourier ridges of filtered BLDCM (with dynamic eccentricity) stator current and 3-Hz sine speed reference.

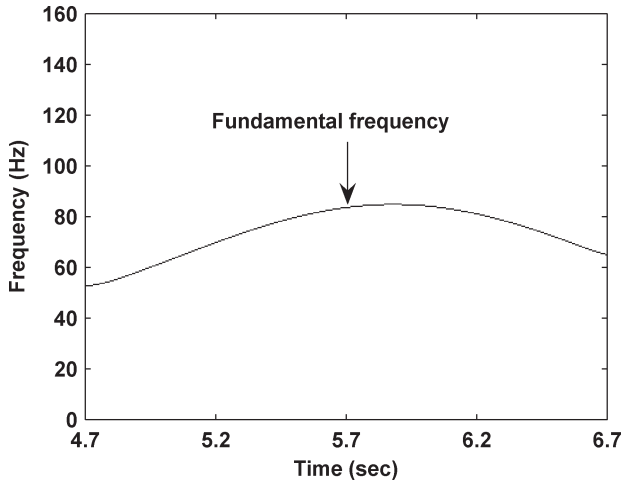

Fig. 15. Windowed Fourier ridges of unfiltered BLDCM (with dynamic eccentricity) stator current and 3-Hz sine speed reference.

The WFRs for a faulty BLDCM operating with a 6-Hz sinusoidal speed reference and an 8-Hz triangular speed reference are shown in Figs. 16 and 17. In both cases, the fault frequencies are again distinctly tracked over time. The fault ridges in Figs. 16 and 17 are identified as BLDCM fault frequencies from the Fourier ridges of the corresponding unfiltered current waveforms as explained previously but are not shown here because of the lack of space.

To validate the effectiveness of the algorithm, the BLDCM with dynamic eccentricity is now operated with a speed reference signal that changes randomly. The nonstationary stator current and the spectrogram of the filtered stator current computed using (4) are shown in Fig. 18. The spectrogram does not clearly depict the instantaneous fault frequencies in the filtered current signal. The WFRs are then extracted from the local maxima of the spectrogram (Fig. 19). Fig. 19 shows that the fault frequencies are distinctly tracked over time. The random changes in the frequencies of the signal are now clearly visible in Fig. 19. This demonstrates the effectiveness of the WFR algorithm to track faults over all types of nonstationary conditions.

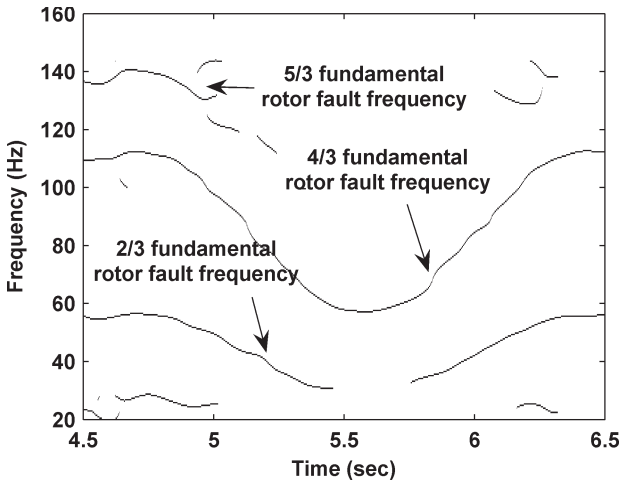

Fig. 16. Windowed Fourier ridges of filtered BLDCM (with dynamic eccentricity) stator current and 6-Hz sine speed reference.

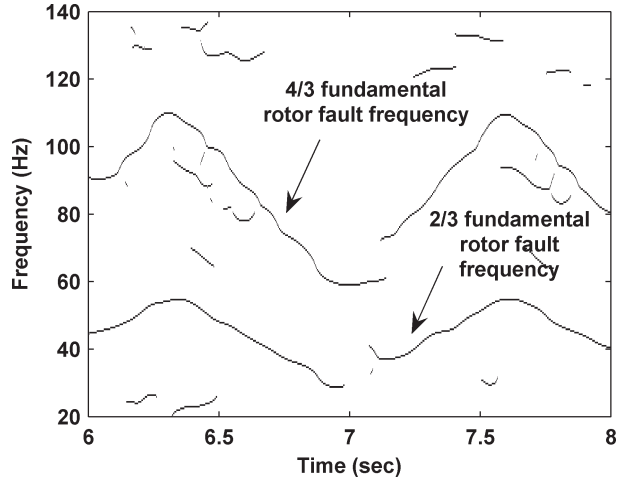

Fig. 17. Windowed Fourier ridges of filtered BLDCM (with dynamic eccentricity) stator current and 8-Hz triangular speed reference.

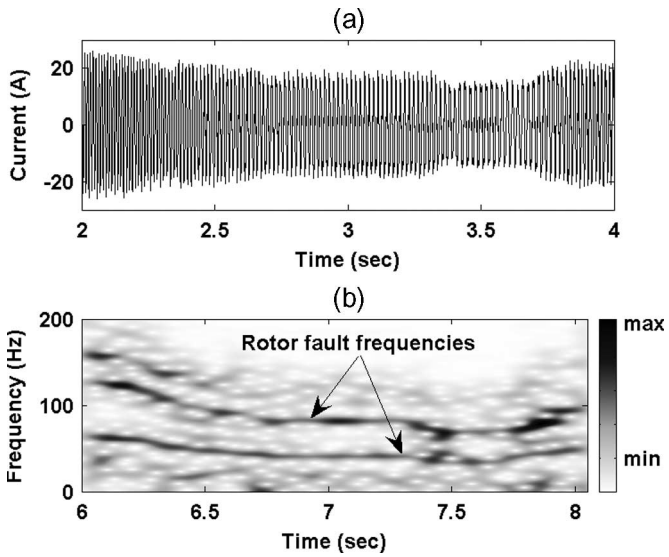

Fig. 18. Nonstationary BLDCM stator current and spectrogram of corresponding filtered BLDCM (with dynamic eccentricity) stator current with random speed reference.

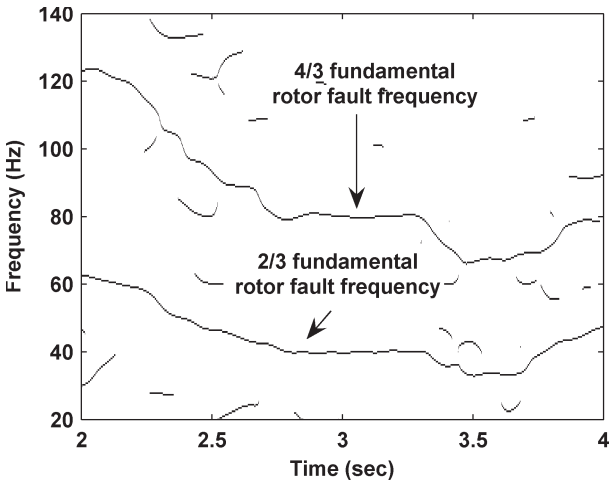

Fig. 19. Windowed Fourier ridges of filtered BLDCM (with dynamic eccentricity) stator current and random speed reference.

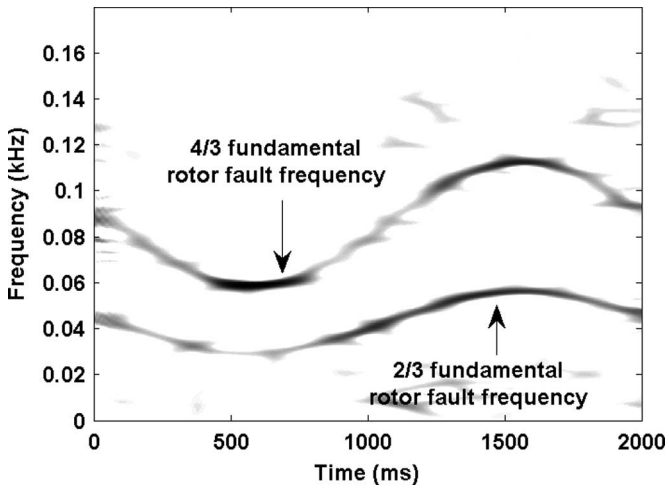

Fig. 20. SPWVD of BLDCM with dynamic eccentricity (5-Hz sinusoidal speed reference).

Method 2 comprising of the SPWVD-based fault detection method is also applied, and some experimental results are shown in this paper. The data are again sampled at 2 kHz. A Hamming smoothing window is chosen. A window of length 0.25 s is used to facilitate a fair comparison with method 1. However, the length or type of the window does not impact the frequency extraction significantly as the WVD-based methods are not sensitive to the window. The length of the time-smoothing Hamming window is 411 samples, and the length of the frequency-smoothing Hamming window is 513 samples. The rotor fault frequencies for the dynamically eccentric motor have been extracted using the SPWVD and are shown in Fig. 20 for the case of $f_{\rm ref} = 5$ Hz. The $t-f$ plot clearly shows the ability of the SPWVD-based methods to extract the fault frequencies over time.

VII. Fault Classification Using RMS Fault Metric

A simple fault metric is computed by calculating the RMS of the fault ridge amplitudes using (19) extracted from the spectrogram/SPWVD of the filtered stator current for a motor speed. Fig. 21 shows the fault metrics calculated for

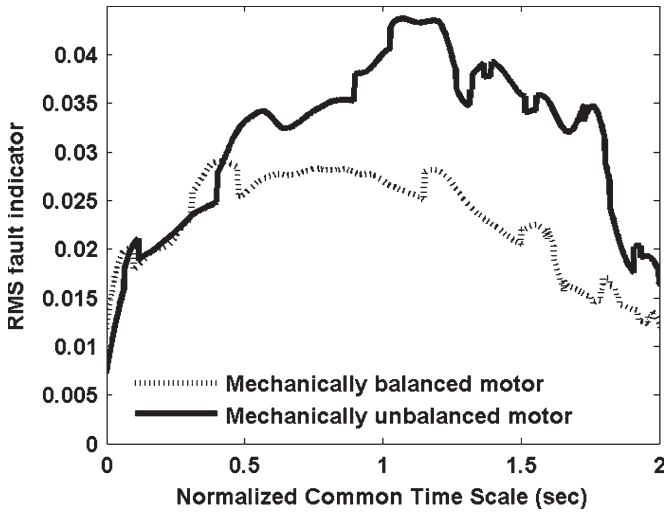

Fig. 21. RMS fault indicator discriminates BLDC rotor unbalance (3-Hz sine speed reference).

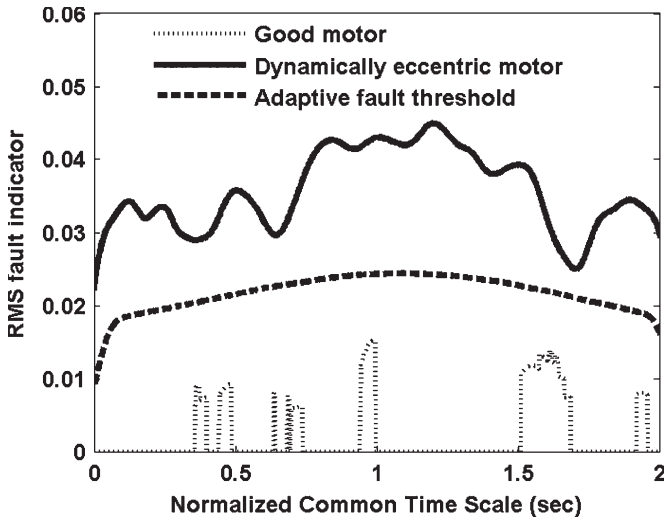

Fig. 22. Detecting dynamic eccentricity with adaptive threshold set at 2% of the fundamental amplitude (3-Hz sine speed reference).

mechanically balanced and unbalanced motors using the instantaneous RMS of the fault ridge amplitudes (Figs. 14, 16, and 17) extracted from the spectrogram of the filtered stator current. A clear change can be seen in the fault metric of the mechanically unbalanced motor, which indicates a fault condition. This fault metric can be used along with a predetermined threshold as an indicator for automatic detection of rotor faults in BLDCMs. More sophisticated fault classifiers using pattern recognition techniques can also be used if needed [25].

The fault metric computed for both a motor with dynamic eccentricity and a good motor are shown for two different time segments in Figs. 22 and 23. The timescales are normalized to obtain a common base for comparison and, therefore, represent a time from 0 to 2 s. A significant difference in the fault metrics of the good and the faulty motor cases is seen. The fault is automatically detected by setting a threshold.

As the motor's operating conditions, namely the speed and the load, vary continuously over time, the amplitudes of the fault frequency components vary, too. For this reason, a

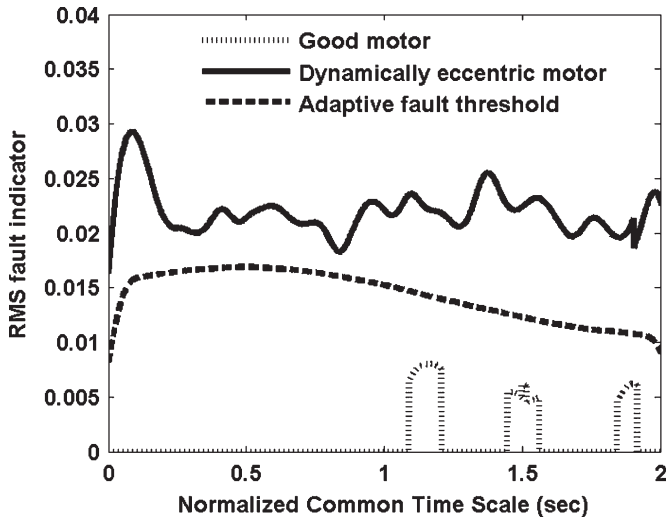

Fig. 23. Detecting dynamic eccentricity with adaptive threshold set at 2% of the fundamental amplitude (3-Hz sine speed reference) for time segment different from Fig. 22.

threshold that can adapt to instantaneous operating conditions is needed for fault discrimination in motors operating under nonstationary conditions. An adaptive heuristic threshold that varies as 2% of the amplitude (21) of the fundamental frequency is shown in Figs. 22 and 23. The amplitude of the fundamental frequency is obtained from the Fourier ridges of the unfiltered signal similar to the one shown in Fig. 15. This threshold is unique to each application and each motor. That is

$$\text{Adaptive threshold} = 0.02 \times \text{Amplitude}[FRi_{\text{aunf}}] \tag{21}$$

where FRi_{aunf} is the Fourier ridge of unfiltered BLDC current computed from the local maxima of the spectrogram using (4)/PWVD or SPWVD calculated using (10)/(11).

VIII. Real-Time Implementation of WVD and WFR

The most important factor in designing any real-time signal processor is the computational load. The spectrogram (WFR) and the WVD are compared for their suitability for implementation in a commercial system. To this effect, the two algorithms are implemented on an ADSP-21061-SHARC digital signal processor (DSP) operating with a 50-MHz clock and capable of 150 Mflops. The ADSP-21061 is a 32-b floating point processor optimized for high-performance DSP applications. The algorithms are first written in the C language. Discretized versions of the WVD and the WFR are used to study practical computation times. Only a brief description of the actual implementation of these algorithms is provided here as the subject is beyond the scope of this paper.

The discrete PWVD (DWVD) is given by [26]

$$W_X(n, f_t) = 2 \sum_{l=-L}^{l=L} s(n+l)s^*(n-l)w_t(l)w_t^*(-l)e^{-4\pi jl} \tag{22}$$

where the value of L is chosen such that $2L+1$ is the length of the signal, w_t is the chosen window function, $f_t(=\omega/2\pi)$ is the

TABLE I
COMPUTATION TIME FOR WFR AND PWVD

Method	Computation time per time slice (μ-sec)
Spectrogram	0.46
WVD	2.02

instantaneous frequency, and n is the time sample. The DWVD can be optimally implemented by evaluating at time zero and shifting the signal $s(n)$ so that time n is mapped to the time origin. This is given by

$$W_X(0, f_t) = 2 \sum_{l=-L}^{l=L} K(l) e^{-4\pi j l} \tag{23}$$

where $K(l)$ is called the DWVD kernel sequence, which is given by

$$K(l) = s(l) s^*(l) w_t(l) w_t^*(-l). \tag{24}$$

The Hilbert transform used to convert the real-valued current signal to an analytic signal is implemented as a 79-tap finite-impulse response filter [26]. The kernel sequence is first computed, and then the DFT is computed to obtain the DWVD of the sequence. The implementation of these algorithms can be found in more detail in [27] and [28].

The WFR method is implemented using the standard DFT and has been implemented by some of the authors of this paper in previous research [29].

The computational load for one time slice of data processed is measured on an oscilloscope and is compared in Table I. The data are divided into bins of 1024 samples, and each bin comprises a time slice. A 512-point FFT is used to compute both the PWVD and the spectrogram (WFR). The spectrogram is implemented using a Gaussian window of length of 0.0625 s (512 samples). The length of the window is chosen heuristically to best fit this application. The PWVD takes almost four times the computation time of the spectrogram, thus demonstrating that the WFR method is computationally less intensive. However, if a high-frequency resolution (low-frequency motor operation) is needed, the WVD-based methods can still be used effectively, provided that sufficient computational capability is available on the signal processor. Moreover, as motor diagnostics are performed over long intervals of time, the computation time may not be critical, and therefore, the WVD-based algorithms can be effectively used.

IX. COMMENTS ON USE OF PROPOSED ALGORITHMS

A. Effective Range of Operation

During the experiments in Section VI, it has been noted that the ridge algorithm is able to extract frequencies from the motor stator current up to a sinusoidal speed reference of 15 Hz and a triangular speed reference of 10 Hz. This range of operation includes robotic actuator applications. The application investigated in this paper is an automotive actuator application, which is similar to robotic applications. The large mechanical time constants of electric motors and loads result in a slow response even during sudden changes in operating conditions. Hence, the frequency information is still preserved in the nonstationary electrical signal. However, beyond the speed reference rates of 15 Hz, the current is extremely nonstationary (especially with a triangular reference) and no longer possesses any instantaneous frequency. However, such nonstationarity does not commonly occur in motor applications.

B. Effect of Load Conditions

The proposed algorithms are tested under widely varying load conditions ranging from low load to full load. The rms fault indicator depicts the strong variation in the amplitude of the fault frequency components. This variation occurs because the load change is directly proportional to speed and, hence, verifies the ability of the fault detection algorithms to work under varied load conditions.

C. Application to Other Rotor Faults

While the cases of unbalanced rotor and dynamic eccentricity have been investigated in this paper, the proposed fault detection methods can be extended to several other rotor faults that create unique fault frequency signatures in the stator current spectrum. These faults included mixed eccentricity (combined dynamic and static eccentricity), broken rotor faults in induction motors, bearing defects, and load-related defects such as gear faults and coupling misalignments. These faults create unique fault frequencies that have been extensively documented [2]–[4]. The implementation of all these faults is, however, beyond the scope of this paper.

D. Application to Motors With Uneven-Asymmetric Rotor Magnetization and Unbalanced Radial Forces

The proposed algorithms can be applied to motors with uneven-asymmetric rotor magnetization (caused, for example, by the use in the same motor of magnets from different production batches) and motors with unbalanced radial forces (such as in a three-phase nine-slot eight-pole design). In both these cases, the frequency spectrum of the stator current of a normal motor would possess the fault frequency components indicated by (1). Prior to commissioning these motors, the amplitudes of all these fault-related frequencies have to be measured. When the motor is commissioned, the proposed algorithms track these fault frequency components and look for abnormal (significant) changes in the amplitudes of these signals over time. A significant change in the amplitude of the fault frequencies would indicate that the motor is developing a rotor fault.

E. Comment of Influence of Inverter Noise, Frequency Resolution, and Sampling Frequency

The inverter switching frequency related noise does not have an impact on the performance of the algorithm, as this noise

is more than a decade above the fundamental frequency and is filtered out using the ATF prior to application of the algorithm. The frequency resolution depends on the sampling frequency and on the amount of samples used for the transformation, that is, if the number of samples multiplied by the sampling frequency is one, the frequency resolution is 1 Hz; if the product is two, the resolution is 0.5 Hz; and so on. The sampling frequency and the number of samples are thus chosen as a tradeoff between the desired frequency resolution for a particular diagnostics problem and the computational capability available with the DSP.

X. Conclusion

The problem and solution to diagnosing rotor faults in BLDCMs operating under continuous nonstationary operation is presented in this paper. The WFRs and WVDs are proposed as novel solutions. WFRs are the local maxima computed from the spectrogram of a nonstationary signal. The Fourier ridges can be detected for maxima of comparable magnitude in multicomponent signals. The WVD-based variants are more complex signal processing techniques that have better frequency resolution characteristics and are inherently suited to nonstationary signals. The methods are not limited to BLDCMs but can be applied to other motors as well.

The ability of the method to detect BLDCM rotor faults such as unbalanced rotors and dynamic eccentricities in various cases of nonstationarity has been demonstrated. The WFR algorithm is unfortunately dependent on the type and length of the data window as it has to be chosen as a tradeoff between time and frequency resolution. However, the method is simple to implement in real time. It is also computationally less intensive than other methods such as WVDs. However, the WVDs have better frequency resolution and are more suitable for motors that exhibit nonstationary operation at low frequencies, too. A simple fault metric based on the RMS of the extracted fault frequencies has been proposed for automatic fault detection. Although validated here on a single test motor, this fault classification could apply to other motors using a threshold that is set heuristically or using sophisticated pattern recognition techniques such as artificial neural networks.

Acknowledgment

The authors would like to thank Delphi Corporation, Troy, MI, and, in particular, Dr. T. Sebastian (Delphi Saginaw Steering Systems), Dr. B. Lequesne, and Dr. T. W. Nehl (Delphi Research Laboratories).

References

[1] M. H. Hayes, *Statistical Digital Signal Processing and Modeling*. New York: Wiley, 1996.

[2] S. Nandi and H. A. Toliyat, "Condition monitoring and fault diagnosis of electrical machines—A review," in *Proc. 34th Annu. Meeting IEEE Ind. Appl.*, 1999, pp. 197–204.

[3] J. M. Cameron, W. T. Thomson, and A. B. Dow, "Vibration and current monitoring for detecting airgap eccentricity in large induction motors," *Proc. Inst. Electr. Eng.*, vol. 133, no. 3, pp. 155–163, 1986.

[4] G. B. Kliman and J. Stein, "Methods of motor current signature analysis," *Electr. Mach. Power Syst.*, vol. 20, no. 5, pp. 463–474, Sep. 1992.

[5] B. Yazici and G. B. Kliman, "An adaptive statistical time–frequency method for detection of broken bars and bearing faults in motors using stator current," *IEEE Trans. Ind. Appl.*, vol. 35, no. 2, pp. 442–452, Mar. 1999.

[6] K. Kim and A. G. Parlos, "Induction motor fault diagnosis based on neuropredictors and wavelet signal processing," *IEEE/ASME Trans. Mechatronics*, vol. 7, no. 2, pp. 201–219, Jun. 2002.

[7] C. Combastel, S. Lesecq, S. Petropol, and S. Gentil, "Model-based and wavelet approaches to induction motor on-line fault detection," *Control Eng. Pract.*, vol. 10, no. 5, pp. 493–509, May 2002.

[8] H. Douglas, P. Pillay, and A. K. Ziarani, "A new algorithm for transient motor current signature analysis using wavelets," *IEEE Trans. Ind. Appl.*, vol. 40, no. 5, pp. 1361–1368, Sep./Oct. 2004.

[9] B. A. Paya, I. I. Esat, and M. N. M. Badi, "Artificial neural network based fault diagnostics of rotating machinery using wavelet transforms as a preprocessor," *Mech. Syst. Signal Process.*, vol. 11, no. 5, pp. 751–765, Sep. 1997.

[10] R. Burnett, J. F. Watson, and S. Elder, "The application of modern signal processing techniques for use in rotor fault detection and location within three-phase induction motors," in *Proc. IEEE IMTC*, 1995, pp. 426–431.

[11] L. Eren and M. J. Devaney, "Motor bearing damage detection via wavelet analysis of the starting current transient," in *Proc. 18th IEEE IMTC*, 2001, pp. 1797–1800.

[12] S. Rajagopalan, W. le Roux, R. G. Harley, and T. G. Habetler, "Diagnosis of potential rotor faults in brushless dc machines," in *Proc. 2nd Int. Conf. PEMD*, 2004, pp. 668–673.

[13] D. G. Dorell, W. T. Thomson, and S. Roach, "Analysis of airgap flux, current, and vibration signals as a function of the combination of static and dynamic airgap eccentricity in 3-phase induction motors," *IEEE Trans. Ind. Appl.*, vol. 33, no. 1, pp. 24–34, Jan./Feb. 1997.

[14] S. Mallat, *A Wavelet Tour of Signal Processing*. San Diego, CA: Academic, 1999, pp. 84–88. 102-107.

[15] N. Delprat, B. Escudie, P. Guillemain, R. Kroland-Martinet, P. Tchamitchian, and B. Torresani, "Asymptotic wavelets and Gabor analysis: Extraction of instantaneous frequencies," *IEEE Trans. Inf. Theory*, vol. 38, no. 2, pp. 644–664, Mar. 1992.

[16] L. Cohen, "Time–frequency distributions—A review," *Proc. IEEE*, vol. 77, no. 7, pp. 941–981, Jul. 1989.

[17] T. A. C. M. Claasen and W. F. G. Mecklenbrauker, "The Wigner distribution—A tool for time–frequency analysis—Part 1: Continuous time signals," *Philips J. Res.*, vol. 35, no. 3, pp. 217–250, 1980.

[18] ——, "The Wigner distribution—A tool for time-frequency analysis—Part 2: Discrete time signals," *Philips J. Res.*, vol. 35, no. 4/5, pp. 276–300, 1980.

[19] B. Boashash, *Time–Frequency Signal Analysis—Methods and Applications*. Melbourne, Australia: Longman Cheshire, 1992.

[20] A. V. Oppenheim, R. W. Schafer, and J. R. Buck, *Discrete-Time Signal Processing*. Englewood Cliffs, NJ: Prentice-Hall, 1999.

[21] L. R. Rabiner and B. Gold, *Theory and Application of Digital Signal Processing*. Englewood Cliffs, NJ: Prentice-Hall, 1975.

[22] F. Auger, P. Flandrin, P. Goncalvès, and O. Lemoine, *Time–Frequency Toolbox for use With MATLAB*. Houston, TX: Rice Univ., 1996.

[23] J. Buckheit, S. Chen, D. Donoho, I. Johnstone, J. Scargle. *Wavelab802 Reference Manual, Ver 0.7000.* (1995). [Online]. Available: http://www-stat.stanford.edu/~wavelab/ftp/WaveLabRef.pdf.Z

[24] P. Bechard. (2004). "Fault zone analysis 'air gap'," *in Proc. Motor Reliab. Tech. Conf.,* pp. 1–7. [Online]. Available: http://www.pdma.com/AirGapFaultZone.pdf

[25] X. Huang, T. G. Habetler, and R. G. Harley, "Detection of rotor eccentricity faults in closed-loop drive-connected induction motors using an artificial neural network," in *Proc. IEEE PESC*, Recife, Brazil, 2004, pp. 913–918.

[26] B. Boashash and P. J. Black, "An efficient real-time implementation of the Wigner–Ville distribution," *IEEE Trans. Acoust., Speech, Signal Process.*, vol. ASSP-35, no. 11, pp. 1611–1618, Nov. 1978.

[27] J. A. Restrepo and P. Bowler, "Analysis of induction machine slot harmonics in the TF domain," in *Proc. 1st IEEE Int. Caracas Conf. Devices, Circuits Syst.*, 1995, pp. 127–130.

[28] J. A. Restrepo, T. Pérez, M. I. Giménez, and V. M. Guzmán, "DSP implementation of an ac-machine sensorless speed measurement system using the Wigner distribution," in *Proc. 7th Eur. Conf. Power Electron. and Appl.*, Trondheim, Norway, 1997, pp. 524–528.

[29] J. M. Aller, T. G. Habetler, R. G. Harley, R. M. Tallam, and S. B. Lee, "Sensorless speed measurement of ac machines using analytic wavelet transform," *IEEE Trans. Ind. Appl.*, vol. 38, no. 5, pp. 1344–1350, Sep./Oct. 2002.

Satish Rajagopalan (S'99–M'01) received the B.E. degree in electrical engineering from the University of Madras, Chennai, India, in 1997, and the M.S.E.E. degree from Iowa State University, Ames, in 2000. His Master's thesis focused on the real-time control of power electronics systems and the use of rapid prototyping and hardware-in-the-loop simulation to speed up the power converter design process. He is currently working toward the Ph.D. degree at the School of Electrical and Computer Engineering, Georgia Institute of Technology, Atlanta.

From 2000 to 2001, he was employed with the Baldor Motors and Drives Inc., Fort Smith, AZ, as a Power Electronics Engineer, where he was involved in the design of electric-motor drives. In 1999, he was a Summer Intern with the Rockwell Collins Inc., Cedar Rapids, IA, where he worked on the design of switching power supplies and electromagnetic-interference suppression filters for aerospace applications.

José M. Aller was born in Caracas, Venezuela, in 1958. He received the B.Ing. degree in electrical engineering from the Universidad Simón Bolívar, Caracas, in 1980, the M.S. degree in electrical engineering from Universidad Central de Venezuela, Caracas, in 1982, and the Ph.D. degree in industrial engineering from Universidad Politécnica de Madrid, Madrid, Spain, in 1993.

He has been a Lecturer with the Universidad Simón Bolívar for 26 years, where he is currently a full-time Professor at the Departamento de Conversión y Transporte de Energía. He was the General Secretary of the Universidad Simón Bolívar between 2001 and 2005. His research interests include space vector application, electrical machine control, and power electronics.

José A. Restrepo (S'89–M'92) received the B.Sc. and M.Sc. degrees in electronics engineering from the Universidad Simón Bolívar, Caracas, Venezuela, in 1988 and 1991, respectively, and the Ph.D. degree from the Institute of Science and Technology, University of Manchester, Manchester, U.K., in 1996.

He is currently a Full Professor of electronics engineering with the Universidad Simón Bolívar. His research interests include advanced control of electrical machines, artificial intelligence, and digital signal processors applied to motion control.

Thomas G. Habetler (S'83–M'83–SM'92–F'02) received the B.S.E.E. and M.S. degrees from the Marquette University, Milwaukee, WI, in 1981 and 1984, respectively, both in electrical engineering, and the Ph.D. degree from the University of Wisconsin—Madison, in 1989.

From 1983 to 1985, he was employed with the Electro-Motive Division of General Motors as a Project Engineer. Since 1989, he has been with the Georgia Institute of Technology, Atlanta, where he is currently a Professor of electrical engineering. His research interests are in electric-machine protection and condition monitoring, and switching converter technology and drives. He has published over 150 papers in these fields. He is a regular consultant to industry in the field of condition-based diagnostics for electrical systems.

Dr. Habetler has received four conference prize paper awards from the Industry Applications Society. He currently serves as IEEE Division II Director-Elect. He is the Past President of the IEEE Power Electronics Society and Past Chair of the Industrial Power Converter Committee of the IEEE Industry Applications Society.

Ronald G. Harley (M'77–SM'86–F'92) received the M.Sc.Eng. degree (*cum laude*) in electrical engineering from the University of Pretoria, Pretoria, South Africa, in 1965 and the Ph.D. degree from the London University, in 1969.

In 1971, he was appointed to the Chair of Electrical Machines and Power Systems at the University of Natal, Durban, South Africa, and later, he became the Department Head and Deputy Dean of Engineering. He is currently the Duke Power Company Distinguished Professor with the Georgia Institute of Technology, Atlanta. His research interests include the dynamic behavior and condition monitoring of electric machines, motor drives, power systems, and their components, and controlling them by the use of power electronics and intelligent control algorithms. He has coauthored some 400 papers and three patents. Altogether, ten of the said papers attracted prizes from journals and conferences.

Dr. Harley is a Fellow of the British IEE. He is also a Fellow of the Royal Society in South Africa and a Founder Member of the Academy of Science in South Africa formed in 1994. During 2000 and 2001, he was one of the IEEE Industry Applications Society's six Distinguished Lecturers. He was the Vice President of Operations of the IEEE Power Electronics Society (2003–2004) and Chair of the Atlanta Chapter of the IEEE Power Engineering Society. He is currently the Publications Chair for IEEE Power Electronics Society, and Chair of the Distinguished Lecturers and Regional Speakers program of the IEEE Industry Applications Society. He received the Cyrill Veinott Award in 2005 from the IEEE Power Engineering Society for "Outstanding contributions to the field of electromechanical energy conversion."